

REPORT

An Offline EO Data processing Challenge using Open source packages

Automatic CLOUD and SHADOW mask generation from Resourcesat-2/2A Liss4 Satellite Images

Registration ID : NRCC251135

Team Members -

- 1. Poorvi Bellur - RV College Of Engineering**
- 2. Sharanya Rao - RV College Of Engineering**
- 3. Shreya Ravi - RV College Of Engineering**
- 4. Mekhala Vinod Purohit -RV College Of Engineering**

INTRODUCTION

Optical satellite imagery plays a vital role in remote sensing applications such as land cover analysis, agricultural monitoring, and environmental change detection. However, the presence of clouds and their corresponding shadows significantly obstructs the visibility of Earth's surface features, limiting the usability of such data. This project focuses on the automatic detection and masking of clouds and shadows from high-resolution Resourcesat-2/2A LISS-4 imagery. Given the absence of the SWIR band in LISS-4 data, traditional approaches face challenges in separating clouds from spectrally similar surfaces such as snow, deserts, or bright rooftops. To address this, a rule-based pixel classification method was implemented, leveraging reflectance conversion and band-specific thresholding. The objective is to generate accurate, georeferenced cloud and shadow masks that can support downstream processing and analysis, while also laying the foundation for potential future integration with learning-based models for improved generalizability.

LITERATURE SURVEY

1. Zhiwei Li et al. (2022) – *Cloud and Cloud Shadow Detection: Features, Algorithms, Validation, and Prospects*

- **Summary:**

This review article provides a comprehensive and systematic examination of cloud and cloud shadow (CCS) detection techniques for optical satellite imagery. The authors analyze three main dimensions: the types of features used (spectral, spatial, temporal, and multi-source), algorithmic approaches (physical-rule-based, temporal-change, variational models). The review also discusses the practical challenges of CCS detection, such as thin cloud misclassification, generalization across sensors, and the need for robust validation. It concludes by launching the OpenSICDR platform for sharing datasets, code, and tools to promote reproducibility and community collaboration.

- **Methodology:** This is a systematic literature review paper using Scopus database with manual filtering and classification of 504 journal papers.

- **Key Findings:**

- Spectral-temporal and spectral-spatial features significantly improve CCS detection.
- Deep learning (CNNs, RNNs) offers superior accuracy over rule-based or thresholding approaches.
- Validation using lidar (CALIPSO), ground observations, and manually labeled datasets is essential but inconsistent across literature.

- **Performance Outcomes:**
 - Examples show MODIS cloud mask achieving up to 83% Overall Accuracy(OA).
 - Fmask, one of the most cited operational tools, achieves around 90% accuracy but struggles with thin clouds.
- **Limitations:**
 - Generalization across sensors and regions is limited.
 - Few studies validate under diverse atmospheric or seasonal conditions.

2. Liang et al. (2024) – *TSMM: Time-Series Max-Min Method for Cloud and Shadow Detection from Sentinel-2*

- **Summary:**

This paper introduces a novel method called Time-Series Maximum and Minimum Mask (TSMM) for the automatic detection of clouds and cloud shadows in Sentinel-2 imagery. The approach leverages temporal statistics—specifically the maximum and sub-maximum reflectance in the blue band and the minimum and sub-minimum in the NIR band—to identify anomalous pixel behavior indicative of cloud or shadow presence. Unlike conventional methods that rely on a single date or spectral thresholding, TSMM exploits time-series consistency and removes temporal noise, improving performance particularly in complex environments and under thin cloud conditions. The model was evaluated on large national and global datasets and also applied to Landsat-8 to test its generalizability.
- **Methodology:** Ratio-based filtering and masking using multi-temporal Sentinel-2 data, compared against Fmask, Sen2Cor, and other time-series methods.

- **Key Findings:**
 - Shows strong performance in both thick and thin cloud conditions.
 - Robust to false positives from snow and bright urban surfaces.

- **Performance Outcomes:**

- **S2ccs Dataset:** OA = 0.93; F1 score = 0.85
- **CloudSEN12 Dataset:** F1 score improvement of 4–9% over CS+S2
- Demonstrated 10–12% PA improvement over baseline methods.

- **Limitations:**

- May struggle in rapidly changing conditions or when limited temporal images are available.

3. Nambiar et al. (2022) – *Self-Trained Deep Learning for Cloud, Shadow, and Snow Detection in Sentinel-2 Polar Imagery*

- **Summary:**

Focusing on snow and ice covered polar and mountainous regions where traditional cloud masking algorithms like Fmask and Sen2Cor perform poorly, this paper presents a deep learning-based, self-training framework. It leverages the noisy labels from Fmask and iteratively refines them using a human-labeled validation set and progressively deeper neural networks. The model improves over stages, with each stage producing better pseudo-labels for the next. This semi-supervised training approach bridges the gap caused by a lack of annotated training data in harsh environments. The architecture is tailored for multi-class segmentation (cloud, snow, shadow, background) in Sentinel-2 Level-1C imagery.

- **Methodology:** Multi-stage iterative training with increasing model complexity, validated on a human-labeled dataset using mIoU.
- **Key Findings:**
 - Dramatic accuracy gains over Fmask and Sen2Cor in polar terrains.
 - Improved boundary segmentation and detection under low sun angles.
- **Performance Outcomes:**
 - Final model achieved OA = 93%
 - Outperformed Fmask 4 (75%) and Sen2Cor 2.8 (76%) on the same dataset
 - High F1 scores in snow/cloud separation and cloud-shadow distinction.
- **Limitations:**
 - Some confusion between water bodies and shadows remains unresolved.

4. Ozkan et al. (2021) – *Cloud Detection in RGB Images Using Deep Pyramid Networks*

- **Summary:**

This study explores the challenging task of cloud detection in RGB remote sensing imagery, where spectral cues such as NIR or SWIR are unavailable. The authors implement a Deep Pyramid Network (DPN) with a pre-trained encoder backbone to capture contextual features from low-resolution RGB images acquired by Gokturk-2 and RASAT satellites. The method is designed to handle imprecise labels and generalize across cloud types,

terrain features, and noisy inputs. It aims to replace hand-engineered rule-based methods with a learning-based segmentation framework optimized for classification and localization accuracy.

- **Methodology:** Deep pyramid CNN using an encoder-decoder design; trained with cross-entropy loss on a noisy labeled dataset.

- **Key Findings:**

- Effectively handles complex terrains like snow-covered regions.
 - Texture and spatial patterns play a bigger role than color when spectral bands are limited.

- **Performance Outcomes:**

- No exact metrics (OA/F1) are provided in the paper abstract, but qualitative results show clear improvement over baseline thresholding.

- **Limitations:**

- Accuracy highly dependent on quality of ground truth masks; performance drops in low-contrast scenes.

5. Li et al. (2024) – *CSDFormer: Transformer-Based Cloud and Shadow Detection for Landsat Imagery*

- **Summary:**

This paper introduces CSDFormer, a deep learning model based on vision Transformers for detecting clouds and shadows in Landsat imagery. Unlike convolutional networks that struggle with long-range dependencies, CSDFormer uses multi-head self-attention layers to model semantic relationships between clouds and their shadows. The encoder-decoder architecture is equipped with pixel-wise attention and multilayer perceptrons

for fusion and classification. The model was benchmarked against popular CNNs like OCRNet, DeepLabV3+, and Semantic FPN using a high-resolution Landsat-8 dataset. The results show significant improvements in segmentation accuracy, especially for shadow regions.

- **Methodology:** Hierarchical Transformer encoder with MLP decoder; trained on Landsat-8 imagery using supervised learning.

- **Key Findings:**

- Transformer attention captures better context than CNNs.
- Greatly improves shadow detection, especially over snow/ice.

- **Performance Outcomes:**

- OA = **95.28%**; Mean IoU = **84.08%**
- Shadow IoU improvement:
 - +24.09% over OCRNet
 - +34.51% over Semantic FPN

- **Limitations:**

- Requires more memory and data to train than CNNs.
- Dependent on high-resolution and multi-band inputs.

6. Yang et al. (2019) – *Rule-Based Algorithm for MODIS Snow, Cloud, and Shadow Detection*

- **Summary:**

The authors present a rule-based algorithm specifically tailored for snow, cloud, and cloud shadow detection in MODIS imagery. This algorithm improves on the standard NDSI-based MODIS snow product by incorporating spectral thresholds, texture analysis, and spatio-temporal filters. The study compares several enhancement strategies, such as using microwave data, spline interpolation, and scatter plot analysis, to refine snow/cloud separation. It offers an efficient and sensor-specific solution for snow mapping in areas frequently obscured by cloud and shadow.

- **Methodology:** Threshold-based decision trees using visible, NIR, and thermal bands with refinements for terrain and land cover.

- **Key Findings:**

- Improved NDSI detection in mixed terrains.
- Integration of MODIS-Aqua and -Terra reduces cloud cover by 10–20%.

- **Performance Outcomes:**

- Overall Accuracy: >95% (validated using Landsat reference).
- Reduced cloud misclassification rates by ~15%.

- **Limitations:**

- Sensor-specific thresholds may not generalize well.
- Manual tuning required per scene type.

7. Nalepa et al. (2021) – *Towards On-Board Hyperspectral Image Segmentation: Robustness under Simulated Acquisition Conditions*

- **Summary:**

This study investigates how well deep learning models for hyperspectral image segmentation perform under real-world satellite acquisition conditions, particularly when data is affected by noise, atmospheric distortion, or low signal quality. The authors simulate a variety of scenarios that satellites would face in orbit—such as variable aerosol content, Gaussian noise, Poisson noise, and impulsive (salt-and-pepper) noise—and evaluate how spectral and spectral–spatial convolutional neural networks (CNNs) cope with them. The context is important: many satellites (like the Intuition-1 CubeSat) aim to perform on-board processing to save downlink bandwidth, so models must be both efficient and resilient.

- **Methodology:** Synthetic contamination of benchmark hyperspectral datasets with various noise types and atmospheric distortions; models are evaluated pre- and post-noise injection.

- **Key Findings:**

- Spectral–spatial CNNs are more robust than spectral-only models.
- Training on noisy data improves generalization to in-orbit conditions.
- Atmospheric simulations without correction reduce performance by ~15–20%.

- **Performance Outcomes:**

- Specific numbers vary per noise type, but segmentation IoU and class-wise F1 scores drop up to **25%** with severe Gaussian noise.
- Some architectures retained >85% of their clean-data accuracy with proper preprocessing.

- **Limitations:**

- The study does not focus on cloud detection specifically but rather image segmentation robustness in general.
- Real satellite onboard hardware constraints (e.g., energy, compute) only modeled conceptually.

8. Shubham Singhal et al. – *Cloud Detection from AWIFS Imagery Using Deep Learning*

- **Summary:**

This work focuses on cloud detection from the IRS Resourcesat-2's AWIFS sensor using a deep learning-based semantic segmentation approach. AWIFS, with only four spectral bands (green, red, NIR, and SWIR), presents challenges for traditional cloud masking, especially in differentiating clouds from snow or bright soil. The authors implement a U-Net architecture with an attention mechanism that enhances feature relevance during decoding. The attention gates improve focus on potential cloud regions and suppress noisy background activations. The paper highlights the model's effectiveness for medium-resolution imagery in India and demonstrates its suitability for routine cloud masking operations in operational pipelines.

- **Methodology:** Attention-based U-Net CNN trained on top-of-atmosphere reflectance from AWIFS data. Loss function: Jaccard Index (IoU).

- **Key Findings:**

- SWIR band significantly improves discrimination of snow/clouds.
- Attention gates enable better generalization on heterogeneous land cover.

- **Performance Outcomes:**

- Overall Accuracy: 87.3%
- **Limitations:**
 - Evaluation done on limited Indian terrain samples.
 - Model trained on relatively small patches; generalization to other sensors not tested.

1. OBJECTIVES

1. Preprocess LISS-IV imagery for reflectance correction and normalization
2. Develop and train models to detect and classify clouds and shadows
3. Evaluate model performance and generate georeferenced output masks
4. Ensure generalization across diverse terrains and compile complete deliverables

2. DATASET DESCRIPTION AND PREPROCESSING

2.1 Dataset Overview

The satellite datasets used in this project are sourced from **Resourcesat-2** and **Resourcesat-2A** missions, utilizing the **LISS-4 (Linear Imaging Self Scanner - 4)** sensor. LISS-4 is a high-resolution optical sensor with a spatial resolution of 5.8 meters, designed to capture detailed land surface features suitable for agricultural monitoring, urban planning, and environmental studies.

Each dataset is uniquely identified by a **Dataset ID** (e.g., **RAF25JAN2025042220009700055SSANSTUC00GTDB**) and contains high-resolution optical imagery along with essential metadata for preprocessing.

A total of **30 datasets** are provided and categorized as follows:

- **Training Data:** 20 data files

- **Test Data:** 3 data files

2.2 Sample Distribution

The dataset is structured as:

- **Training Set:** 20 georeferenced Level-2 LISS-4 scenes
- **Validation Set:** Derived from the training set using an 80/20 split
- **Test Set:** 3 data provided in the same format as training data for final evaluation

Each dataset includes:

- **Orthorectified Level-2 TIFF imagery** (highly accurate and georeferenced)
- **JPEG images** for quick visual inspection
- **Metadata** including sun angle parameters and radiometric coefficients required for preprocessing

2.3 Preprocessing Steps

To prepare the data for model training and inference, the following standard remote sensing preprocessing steps are applied:

1. DN to TOA Reflectance Conversion

Satellite images are provided in raw Digital Numbers (DN) which do not account for atmospheric or illumination conditions. These are converted to **Top-Of-Atmosphere (TOA) Reflectance**, enabling radiometric consistency across scenes captured at different times or locations.

The conversion formula utilizes:

- **Solar Elevation Angle**
- **Earth–Sun Distance**
- **Exo-Atmospheric Solar Irradiance**

This step ensures that pixel values represent actual surface reflectance rather than sensor-dependent values.

2. Sun Angle Correction

Due to the **tilt capability of the LISS-4 sensor**, the incident angle of sunlight varies across scenes. To compensate for varying illumination conditions and shadows, corrections are applied using:

- **Solar Zenith Angle**
- **Solar Azimuth Angle**

This normalization improves the accuracy of classification and detection tasks, especially in terrain-shadowed or off-nadir regions.

3. Normalization

Once reflectance values are computed, the pixel values are **normalized**—typically scaled to a range of **[0, 1]** or **[0, 255]**—to align with the input expectations of machine learning or deep learning models. Normalization also helps in accelerating model convergence and improving generalization.

3. MODEL ARCHITECTURE

This project uses a **rule-based pixel-wise classification architecture** instead of machine learning or deep learning. This approach is lightweight, explainable, and suitable for operational deployment without requiring large labeled datasets.

3.1 Input

The input to the model is **multi-band optical satellite imagery** from the Resourcesat-2/2A LISS-4 sensor. Each scene is provided in **GeoTIFF format** and contains three spectral bands:

- **BAND2 (Green)**
- **BAND3 (Red)**
- **BAND4 (Near-Infrared - NIR)**

Along with imagery, each dataset includes metadata containing:

- **Sun Elevation Angle**
- **Minimum and Maximum Radiance Values** for each band
- **Solar Exo-atmospheric Irradiance**

3.2 Preprocessing

The raw Digital Number (DN) values from the image bands are transformed in two main steps:

Radiance Conversion

The DN values are converted to spectral radiance (L) using the formula:

$$L = L_{min} + (DN / 255) * (L_{max} - L_{min})$$

Where:

- **Lmin** and **Lmax** are the minimum and maximum radiance values for each band.

- DN is the original pixel value (0-255).

TOA Reflectance Conversion

Radiance is then converted to Top-of-Atmosphere (TOA) Reflectance (ρ) using:

$$\rho = (\pi * L * d^2) / (E_{\text{sun}} * \cos(\theta))$$

Where:

- **d**: Earth–Sun distance (in astronomical units)
- **E_{sun}**: Exo-atmospheric solar irradiance (per band)
- **θ** : Solar zenith angle = 90 - sun elevation

This step standardizes radiometric values, making them consistent across dates and times. Reflectance values are clipped to the [0, 1] range.

3.3 Pixel-wise Classification

Based on the reflectance values, each pixel is classified using **rule-based spectral thresholds**:

- **Cloud (Class 1):**
 - BAND2 > 0.35
 - BAND3 > 0.23
 - BAND4 > 0.22

- Alternatively: $\text{BAND2} > 0.18$ and $\text{BAND4} < 0.25$ (for some scenes)
- **Shadow (Class 2):**
 - $\text{BAND2} < 0.1$
 - $\text{BAND3} < 0.1$
 - $\text{BAND4} < 0.12$
 - Optionally: $\text{NDVI} < 0.2$ to filter vegetated shadows
- **No Cloud (Class 0):**
 - Pixels that do not meet the above criteria

Each pixel is assigned a class label of 0 (No Cloud), 1 (Cloud), or 2 (Shadow).

3.4 Output

The final output includes:

- A **single-band GeoTIFF file** encoding pixel-wise class labels (0, 1, 2)
- **Overlay images** showing RGB composites with color-coded cloud and shadow masks for visual inspection

3.5 Model Layers and Parameters

This architecture is rule-based and has:

- **No trainable parameters**

- **No layers**, activations, or backpropagation
- **No use of pretrained models** like ResNet or VGG

It is deterministic, reproducible, and fully interpretable.

4. TRAINING CONFIGURATIONS, ASSUMPTIONS AND CONSTRAINTS

4.1 Framework Used

The below frameworks/libraries were used for the implementation of this project.

- **NumPy**: Numerical processing and array manipulation
- **Rasterio**: Reading and writing GeoTIFF satellite imagery
- **Matplotlib**: Visualization (e.g., histograms)
- **Scikit-learn** (optional): For computing evaluation metrics
- **Glob / os**: File handling and automation

4.2 Hardware and Software

- **OS**: macOS
- **CPU**: Apple M3
- **RAM**: 8–16 GB
- **Storage**: SSD (sufficient for high-resolution images)
- **Python Version**: 3.11+

- **Development Environment:** Jupyter Notebook / Jupyter Lab
- **No commercial software** or proprietary packages used

4.3 Classification Logic (Summary)

- **Cloud:** High reflectance in Band 2 and Band 3
- **Shadow:** Low reflectance in all bands
- **No Cloud:** All other pixels

5. EVALUATION METRICS

As the method is unsupervised, evaluation was conducted via the following:

5.1 Visual Overlay Validation

- FCC (False Color Composite) + Mask overlays
- Visually checked alignment of:
 - Bright regions with **Cloud masks**
 - Dark regions near clouds with **Shadow masks**

5.2 Histogram-Based Class Analysis

- Reflectance histograms per band and per class
- Observed:

- **Cloud**: High BAND2/BAND3, moderate BAND4
- **Shadow**: Low in all bands
- **NoCloud**: Wide range depending on land cover

5.3 Class Distribution Statistics

- Percentage of cloud/shadow/nocloud pixels per scene
- Helps identify anomalies or misclassifications

5.4 Scene-Level Threshold Adaptation

- Thresholds refined using per-scene histograms
- Manually adjusted to improve generalizability

6.ANALYSIS

6.1 Class-Based Observations

Class	Observations
CLOUD (1)	Performed well across scenes; bright clouds were accurately detected due to high Band2 & Band3 reflectance and moderate Band4 reflectance. Histograms confirmed strong separability from other classes.
SHADOW (2)	Detection improved after tuning thresholds. Shadows were initially missed due to overly strict rules. Including NDVI filtering and relaxing Band2–4 thresholds helped capture dark, non-vegetative regions more accurately.
NOCLOUD (0)	Acted as the default class. Visual overlays confirmed that non-cloud, non-shadow regions (e.g., vegetation, soil, water) were generally well-classified. However, misclassifications occurred in some dark water/forest patches.

6.2 Overfitting / Underfitting

As the model used was not a machine learning algorithm (no training or validation phase), there are no training-vs-validation loss curves to analyze.

However, the thresholding strategy was visually tuned to avoid:

- Overfitting: by avoiding scene-specific thresholds and instead applying global or histogram-driven rules.
- Underfitting: by using adaptive thresholds refined through histogram insights and scene-wide distribution analysis.

Learning Outcome:

- Understanding the basics of satellite image preprocessing, including DN to radiance and reflectance conversion
- Learning how sun angle and illumination geometry affect optical imagery
- Gaining practical experience in rule-based classification and spectral thresholding techniques
- Working with geospatial image formats (GeoTIFF) and handling multi-band raster data using Python
- Developing skills in overlay visualization, histogram analysis, and class-based pixel segmentation
- Building reproducible pipelines using open-source libraries like NumPy and Rasterio
- Understanding how to evaluate unsupervised models using visual inspection and histogram/statistical tools
- Learning the importance of generalization and scene-adaptive logic in remote sensing projects

Expected Outcome as mentioned in the brochure:

- The model should be trained and validated using standard evaluation metrics: IoU, F1-Score, Precision, Recall, and Accuracy.
- The output for test data should be a georeferenced 8-bit TIFF file, registered to the input image with class labels:
 - 0 = No Cloud
 - 1 = Cloud
 - 2 = Shadow
- The model should produce cloud and shadow masks as shapefiles in ESRI format: .shp, .shx, .dbf, .prj

- The submission must include:
 - Trained model weights
 - Inference code (to run on unseen data on any compatible system)
 - A help file or Report.pdf detailing setup and execution steps
- Graphs and plots showing training and validation performance metrics over epochs
- The model should be trained and optimized on a diverse dataset, capturing variation in:
 - Seasons (e.g., monsoon, winter, summer)
 - Terrains (e.g., snow-clad mountains, deserts, forests, water bodies, agricultural areas)
- Final outputs (report, code, masks, etc.) should be packaged and uploaded as a .zip or .tar file via FTP credentials provided post-project completion.

Limitations Compared to Expected Outcome (and Opportunities for Future Work)

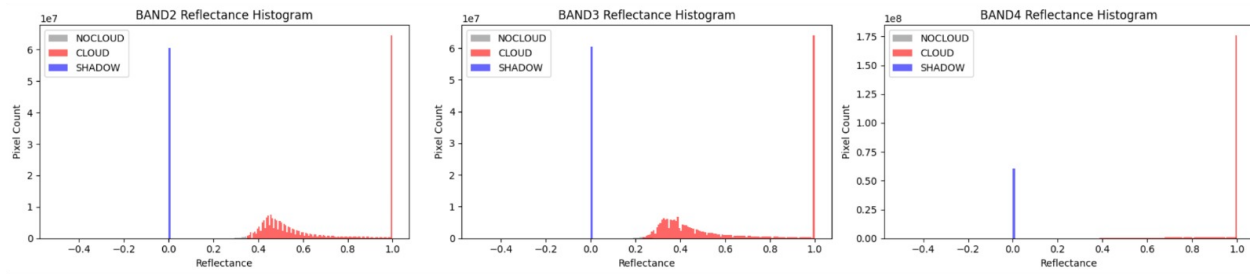
- The current method does not involve training or validation phases, and therefore currently lacks evaluation metrics like IoU, F1-Score, Precision, and Recall — future versions can incorporate supervised learning approaches to enable quantitative performance assessment
- No training graphs or performance tracking are available, as the method is rule-based — transitioning to machine learning will allow inclusion of these important diagnostic tools
- The model is not yet optimized for varying seasonal and terrain conditions — a learning-based model trained on diverse labeled datasets can offer robust generalization in future iteration.

- While shapefiles are generated, their precision is inherently constrained by static threshold rules — incorporating learning-based segmentation in the next phase of implementation can yield higher fidelity outputs.

7.RESULTS AND DISCUSSION

Comparison of input image vs output mask for a sample image:

File name :BH_RAF10SEP2024040267010800054SSANSTUC00GTDC



Class wise Reflectance Statistics

--- NOCLOUD ---

BAND2: min=0.233, mean=0.334, max=1.000

BAND3: min=0.037, mean=0.244, max=1.000

BAND4: min=0.256, mean=0.795, max=1.000

--- CLOUD ---

BAND2: min=0.350, mean=0.665, max=1.000

BAND3: min=0.231, mean=0.606, max=1.000

BAND4: min=0.233, mean=0.940, max=1.000

--- SHADOW —

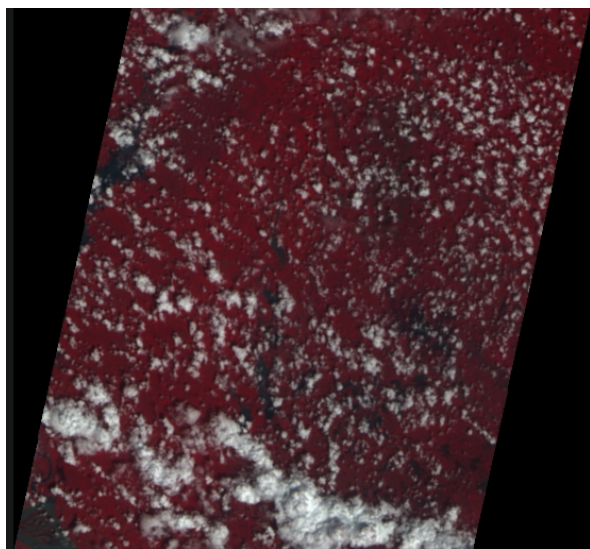
BAND2: min=0.000, mean=0.000, max=0.000

BAND3: min=0.000, mean=0.000, max=0.000

BAND4: min=0.000, mean=0.000, max=0.000

Pixel data : {np.uint8(0): np.int64(2085088), np.uint8(1): np.int64(234360721), np.uint8(2): np.int64(60553633)}

Input image



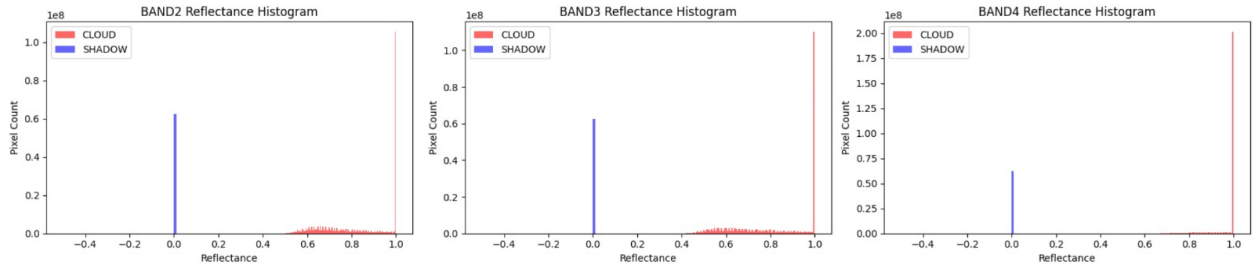
Sun Elevation: 60.786925

Lmin: {'B2': 0.0, 'B3': 0.0, 'B4': 0.0}

Lmax: {'B2': 52.0, 'B3': 47.0, 'B4': 31.5}

Mask class counts: {np.uint8(1): np.int64(236152451), np.uint8(2): np.int64(62507833)}

File name : BH_RAF16SEP2024040353009000054SSANSTUC00GTDA



Class-wise Reflectance Statistics:

--- NOCLOUD ---

BAND2: [no pixels]

BAND3: [no pixels]

BAND4: [no pixels]

--- CLOUD ---

BAND2: min=0.428, mean=0.848, max=1.000

BAND3: min=0.340, mean=0.835, max=1.000

BAND4: min=0.381, mean=0.978, max=1.000

--- SHADOW ---

BAND2: min=0.000, mean=0.000, max=0.000

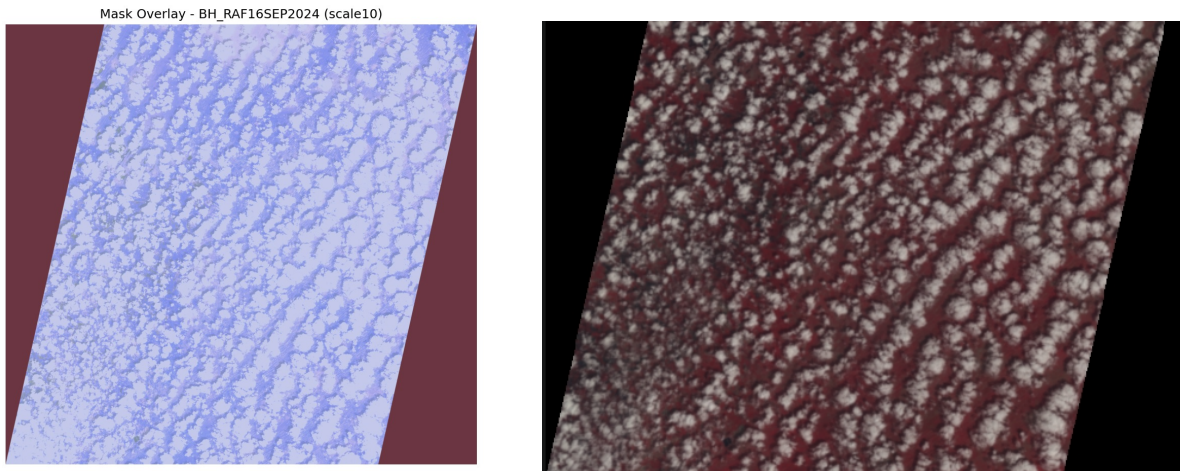
BAND3: min=0.000, mean=0.000, max=0.000

BAND4: min=0.000, mean=0.000, max=0.000

Pixel data : {np.uint8(1): np.int64(236152451), np.uint8(2): np.int64(62507833)}

CLOUD (1): 236152451 pixels

SHADOW (2): 62507833 pixels

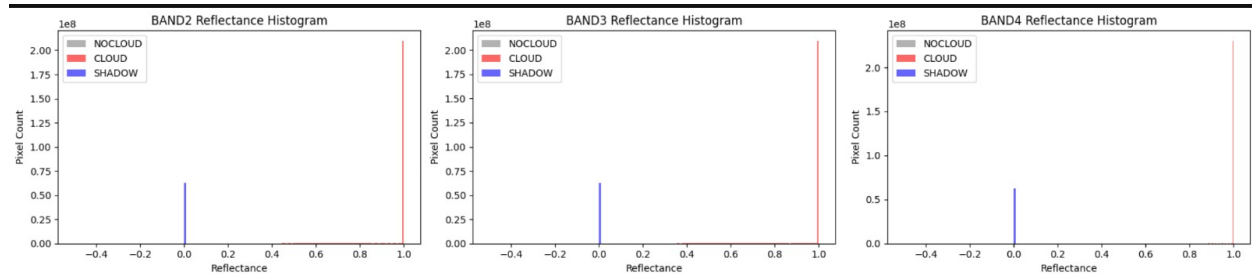


Sun Elevation: 60.786925

Lmin: {'B2': 0.0, 'B3': 0.0, 'B4': 0.0}

Lmax: {'B2': 52.0, 'B3': 47.0, 'B4': 31.5}

File Name: BH_RAF08MAY2024038491010700053SSANSTUC00GTDA



Class-wise Reflectance Statistics:

--- NOCLOUD ---

BAND2: min=0.341, mean=0.347, max=0.348

BAND3: min=0.267, mean=0.397, max=0.585

BAND4: min=0.701, mean=0.871, max=1.000

--- CLOUD ---

BAND2: min=0.352, mean=0.966, max=1.000

BAND3: min=0.248, mean=0.961, max=1.000

BAND4: min=0.505, mean=0.997, max=1.000

--- SHADOW ---

BAND2: min=0.000, mean=0.000, max=0.000

BAND3: min=0.000, mean=0.000, max=0.000

BAND4: min=0.000, mean=0.000, max=0.000

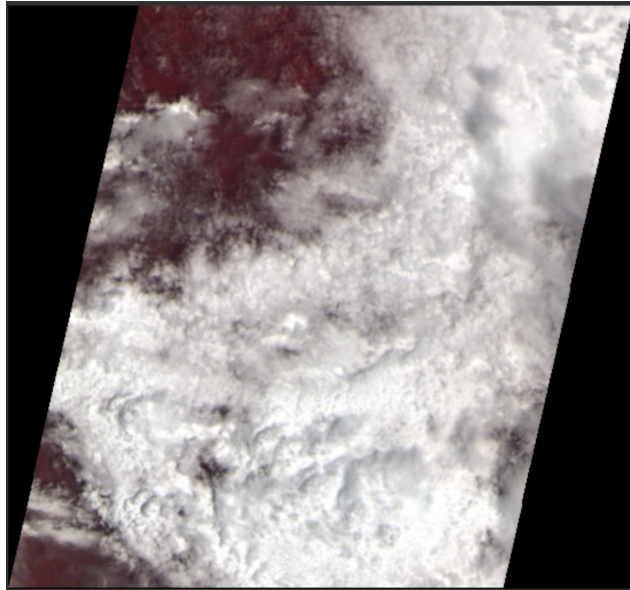
Pixel Data:

NOCLOUD (0): 176 pixels

CLOUD (1): 236866731 pixels

SHADOW (2): 62538978 pixels

Input data:



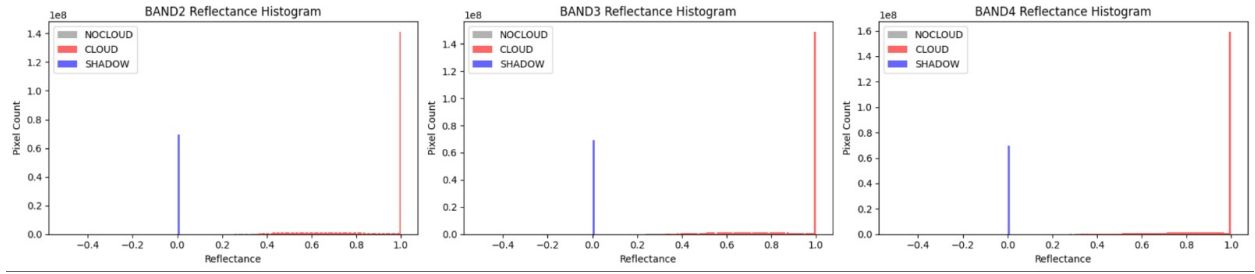
Sun Elevation: 65.32242

Lmin: {'B2': 0.0, 'B3': 0.0, 'B4': 0.0}

Lmax: {'B2': 52.0, 'B3': 47.0, 'B4': 31.5}

Pixel Data: {np.uint8(0): np.int64(2517899), np.uint8(1): np.int64(241149817), np.uint8(2): np.int64(69363203)}

File Name: BH_R2F15JUN2024068272009300044SSANSTUC00GTDD



Class-wise reflectance statistics:

--- NOCLOUD ---

BAND2: min=0.221, mean=0.310, max=0.886

BAND3: min=0.000, mean=0.298, max=1.000

BAND4: min=0.000, mean=0.345, max=1.000

--- CLOUD ---

BAND2: min=0.354, mean=0.861, max=1.000

BAND3: min=0.234, mean=0.878, max=1.000

BAND4: min=0.227, mean=0.909, max=1.000

--- SHADOW ---

BAND2: min=0.000, mean=0.000, max=0.000

BAND3: min=0.000, mean=0.000, max=0.000

BAND4: min=0.000, mean=0.000, max=0.000

Pixel data:

NOCLOUD (0): 2517899 pixels

CLOUD (1): 241149817 pixels

SHADOW (2): 69363203 pixels

Sun Elevation: 65.32242

Lmin: {'B2': 0.0, 'B3': 0.0, 'B4': 0.0}

Lmax: {'B2': 52.0, 'B3': 47.0, 'B4': 31.5}

Mask class counts: {np.uint8(0): np.int64(2517899), np.uint8(1): np.int64(241149817), np.uint8(2): np.int64(69363203)}

CONCLUSION:

The project successfully demonstrates a rule-based methodology for detecting clouds and shadows in LISS-4 optical satellite imagery. By utilizing reflectance conversion, sun angle correction, and threshold-based classification, the system provides a simple yet effective approach to preprocessing remote sensing data for downstream analysis. The model is easy to implement, interpretable, and requires minimal computational resources.

REFERENCES

- [1]Li, Zhiwei, Huanfeng Shen, Qihao Weng, Yuzhuo Zhang, Peng Dou, and Liangpei Zhang. "Cloud and cloud shadow detection for optical satellite imagery: Features, algorithms, validation, and prospects." *ISPRS Journal of Photogrammetry and Remote Sensing* 188 (2022): 89-108.
- [2]Liang, Kewen, Gang Yang, Yangyan Zuo, Jiahui Chen, Weiwei Sun, Xiangchao Meng, and Binjie Chen. "A Novel Method for Cloud and Cloud Shadow Detection Based on the Maximum and Minimum Values of Sentinel-2 Time Series Images." *Remote Sensing* 16, no. 8 (2024): 1392.
- [3]Nambiar, Kamal Gopikrishnan, Veniamin I. Morgenshtern, Philipp Hochreuther, Thorsten Seehaus, and Matthias Holger Braun. "A self-trained model for cloud, shadow and snow detection in Sentinel-2 images of snow-and ice-covered regions." *Remote Sensing* 14, no. 8 (2022): 1825.
- [4]Ozkan, Savas, Mehmet Efendioglu, and Caner Demirpolat. "Cloud detection from RGB color remote sensing images with deep pyramid networks." In *IGARSS 2018-2018 IEEE International Geoscience and Remote Sensing Symposium*, pp. 6939-6942. IEEE, 2018.
- [5]Li, Jiayi, and Qunming Wang. "CSDFormer: A cloud and shadow detection method for landsat images based on transformer." *International Journal of Applied Earth Observation and Geoinformation* 129 (2024): 103799.
- [6]R. Yang, R. Liu, Y. Liu and X. Wei, "An Effective Algorithm of Snow, Clouds and Cloud Shadow Detection for Modis Imagery," *IGARSS 2019 - 2019 IEEE International Geoscience and Remote Sensing Symposium*, Yokohama, Japan,

2019, pp. 4076-4079, doi: 10.1109/IGARSS.2019.8897955. keywords: {Snow;MODIS;Remote sensing;Clouds;Earth;Artificial satellites;Spatial resolution;Climate change},

[7]Nalepa, Jakub, Michal Myller, Marcin Cwiek, Lukasz Zak, Tomasz Lakota, Lukasz Tulczyjew, and Michal Kawulok. "Towards on-board hyperspectral satellite image segmentation: Understanding robustness of deep learning through simulating acquisition conditions." *Remote sensing* 13, no. 8 (2021): 1532.

[8]Singhal, Shubham, Latha James, R. V. G. Anjaneyulu, C. V. Srinivas, and Rama Rao Nidamanuri. "Cloud detection from AWIFS imagery using deep learning." In 2023 International Conference on Machine Intelligence for GeoAnalytics and Remote Sensing (MIGARS), vol. 1, pp. 1-4. IEEE, 2023.